Journal of
Applied
Crystallography
ISSN 0021-8898

Received 25 August 2005
Accepted 22 November 2005

Analytic determination of the three-dimensional distribution of dislocations using synchrotron X-ray topography

J. M. Yi,[a] Y. S. Chu,[b] T. S. Argunova[a,c] and J. H. Je[a]*

[a]Department of Materials Science and Engineering, POSTECH, Pohang 790-784, Korea, [b]Advanced Photon Source, Argonne National Laboratory, IL 60439, USA, and [c]Ioffe Physico-Technical Institute, RAS, St Petersburg, Russian Federation. Correspondence e-mail: jhje@postech.ac.kr

A technique, using a symmetric reflection *via* azimuthal rotation of a sample, is presented for characterization of the three-dimensional distribution of dislocations in single crystals. An analytic formula is derived to transform the three-dimensional geometry of a straight dislocation into its two-dimensional projection onto the detector plane. By fitting topographs to the formula, the orientations and locations of dislocations are quantitatively determined. The dislocations in a thermally stressed Si wafer are examined as an example.

1. Introduction

Characterization of the orientations and locations of dislocation lines in single crystals, together with the Burgers vectors, is an important issue not only for identifying the nature of dislocations, but also for understanding the formation of local microstructure (lattice tilt, strain *etc.*). Some X-ray topographic techniques, such as stereographic techniques in Laue (Lang, 1959*a*,*b*; Haruta, 1965) or Bragg (Vreeland, 1976) geometries, and the 'topo-tomographic' technique (Ludwig *et al.*, 2001), are currently applied for qualitative determination of the orientations and locations of these lines.

On the other hand, recent developments of on-line high-resolution diffraction imaging, activated by using real-time imaging systems in conjunction with synchrotron radiation (Koch *et al.*, 1998), have significantly facilitated the mapping of local microstructure by rocking-curve imaging (Lübbert *et al.*, 2000). A straightforward correlation between the local microstructure and the configuration of the dislocations involved is an issue of interest. For this work, dislocation characterization that is experimentally compatible with the rocking-curve imaging is required.

In this paper, a technique is suggested for quantitative determination of the orientations and locations of dislocation lines in single crystals. The technique is based on using a symmetric reflection of Bragg geometry *via* azimuthal rotation of a sample. As an example, the dislocations in a thermally stressed Si wafer are examined.

2. Experiment

Synchrotron X-ray topography experiments were performed at the XOR 2-BM beamline of the Advanced Photon Source, USA. A monochromatic beam was provided by an Si(111) double-bounce monochromator at 15 keV. A lens-coupled high-resolution CCD camera system was used for imaging diffracted beam intensity. High-resolution imaging was achieved by focusing the visible light, produced by the diffracted beam striking a $CdWO_4$ scintillation crystal, through a 10× objective lens to yield 0.65 μm effective pixel resolution. The CCD system was set up normal to the diffracted beam and positioned 5 mm away from the sample.

As a test sample, an Si(001) wafer, 0.75 mm thick, was employed to characterize the dislocations that were caused by thermal stress during heating of the wafer at 1323 K. The sample was set to a symmetric Si 004 reflection ($\theta = 17.7^\circ$) in the Bragg geometry. In this experiment the 'direct image' was the dominant contrast mechanism, as the bandwidth, $\Delta\lambda/\lambda \simeq 10^{-4}$, of the incoming beam was large compared with the intrinsic width, $\Delta\omega_g^\lambda/\lambda \simeq 10^{-5}$, of the Si 004 reflection (Authier, 2001). The sample was oriented so that the $[1\bar{1}0]$ direction was perpendicular to the scattering plane defined by $\mathbf{k}_i$ and $\mathbf{k}_f$, where $\mathbf{k}_i$ and $\mathbf{k}_f$ are the incident and exit wavevectors, respectively. This angular position was designated as $\phi = 0^\circ$, where ϕ is the azimuthal rotation angle around the diffraction vector $\mathbf{g}$.

A series of X-ray topographs was taken while rotating the azimuthal angle of the sample in 45° steps over a total range of 180°. Any angular step and range would provide a series of topographs, but we have noted empirically that 45° steps in the 180° range is optimum to reduce ambiguities in image analysis. Specifically, the weak-beam technique (Authier, 2001) was applied for each topograph in order to narrow the width of dislocation images and to avoid the double contrast that appeared at the peak of the rocking curve of the sample. The typical exposure time for each topograph was a few seconds.

3. Description of the transformation formula

Since X-ray topography provides a two-dimensional projection of the three-dimensional configuration of a dislocation, it is very useful to formulate the geometrical relation between the configuration in the sample and the topograph (Miltat & Dudley, 1980; Yuan & Dudley, 1992). Fig. 1(*a*) shows a schematic diagram of the transformation of a dislocation configuration by X-ray topography after an azimuthal rotation ϕ of the sample. We define an *xyz* Cartesian coordinate system such that the *z* axis is along the diffraction vector $\mathbf{g}$ and the *yz* plane coincides with the scattering plane. A dislocation line is represented by a vector $\mathbf{u}$,

$$\mathbf{u} = \left[\Gamma\cos\alpha\cos(\beta+\phi),\ \Gamma\cos\alpha\sin(\beta+\phi),\ -\Gamma\sin\alpha\right], \qquad (1)$$

where α and β are two Euler angles at $\phi = 0^\circ$, and Γ is the length of the dislocation. On the other hand, the dislocation line measured in the detector plane is represented by a vector $\mathbf{u}'$,

$$\mathbf{u}' = (\Gamma' \cos\varphi,\ \Gamma' \sin\varphi), \tag{2}$$

in an XY Cartesian coordinate system, where φ is the angle of the line with respect to the X axis and Γ' is the length. In the parallel-beam approximation, $\mathbf{u}'_X = \mathbf{u}_x$. The coordinate transformation of $\mathbf{u}_y$ and $\mathbf{u}_z$ into $\mathbf{u}'_Y$ is easily seen in Fig. 1(*b*), which shows the components of $\mathbf{u}$ on the yz plane and the Y component of $\mathbf{u}'$. It is clear that $\mathbf{u}'_Y$ is equal to the projection of $\mathbf{u}_z$ and $\mathbf{u}_y$ onto the detection plane that is normal to the diffracted beam. Thus, the following relationship holds:

$$\begin{aligned}\mathbf{u}' &= (\Gamma' \cos\varphi, \Gamma' \sin\varphi) \\ &= \left[\Gamma \cos\alpha \cos(\beta+\phi), \Gamma \sin\alpha \cos\theta + \Gamma \cos\alpha \sin(\beta+\phi)\sin\theta\right].\end{aligned} \tag{3}$$

Consequently, we obtain the angular and length components of the transformation formula,

$$\tan\varphi = \tan\alpha \cos\theta / \cos(\beta+\phi) + \tan(\beta+\phi)\sin\theta \tag{4}$$

and

$$\Gamma'^2/\Gamma^2 = \left[\cos(\beta+\phi)\cos\alpha\right]^2 + \left[\sin\theta \sin(\beta+\phi)\cos\alpha + \cos\theta \sin\alpha\right]^2. \tag{5}$$

4. Results and discussion

Fig. 2 shows the series of topographs obtained for the Si 004 reflection by the azimuthal ϕ rotation of the sample. The black lines represent the enhanced intensity of direct dislocation images. The alignment of the dislocations with parallel arrays shows a typical slip-band in a thermally stressed Si wafer. The contrast of the outcrops (surface ends) of the dislocations appears reversed (white or black) between Figs. 2(*a*)–2(*b*) and 2(*d*)–2(*e*) as a result of the exchange of the entrance and exit surfaces by the azimuthal rotation. The variation of the two-dimensional configuration of the lines with the azimuthal rotation shows nonlinear features. For instance, line *A* changes its direction little between $\phi = 0$ and 45°, while the change is drastic after 45°. It is obvious that such nonlinear features result from the projection effect of the three-dimensional characteristics of the dislocations. An analytic approach is preferable to understand this behavior and to determine the configuration of the dislocation lines in the sample.

We performed quantitative analysis on the variation of the two-dimensional configuration of the lines for the three representative dislocation lines, *A*–*C*, and the virtual line (denoted *D*) connecting the two outcrops of *A* and *B* in Fig. 2. The angles (φ) with respect to the horizontal X axis and the projected lengths (Γ') (for *B* and *D*) were measured by indexing two XY points of each line using image analysis software. Figs. 3(*a*) and 3(*b*) represent the variation of the angles and the lengths, respectively, as a function of the azimuthal rotation angles. The data obtained were fitted to the transformation formulae [equations (4) and (5)] by the least-squares method, as indicated by the solid lines in the figures. The two fitting parameters, α

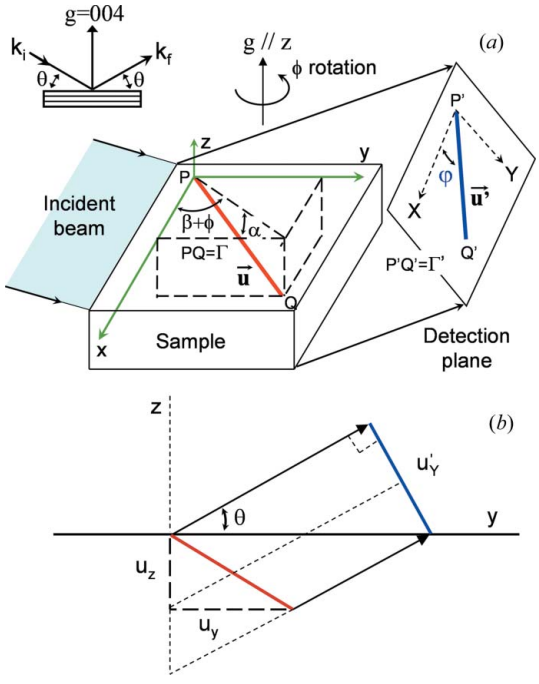

Figure 1
(*a*) A schematic diagram of the transformation of a dislocation line ($\mathbf{u}$) into its two-dimensional projection ($\mathbf{u}'$). Dotted lines define the sample volume illuminated by X-rays. The inset in the top-left of the figure shows the geometry of the experiment. (*b*) A schematic diagram of the components of $\mathbf{u}$ on the yz plane and the Y component of $\mathbf{u}'$.

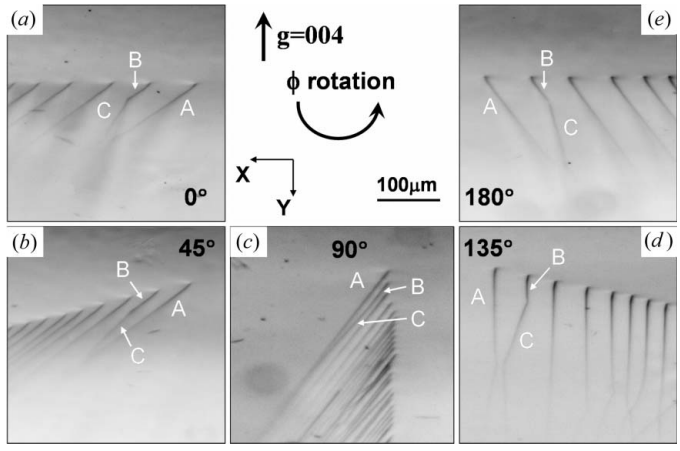

Figure 2
A series of X-ray topographs, obtained from the Si 004 reflection *via* the azimuthal rotation of the sample. Three representative dislocations, *A*–*C*, are indicated in each topograph. The rotation angles are marked.

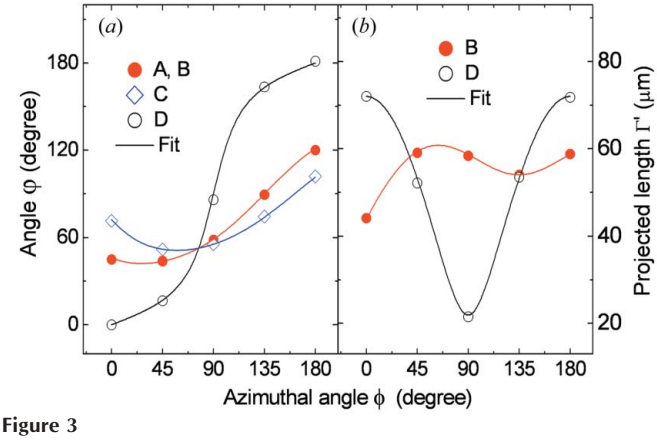

Figure 3
The variation of (*a*) the angles φ and (*b*) the projected lengths Γ' as a function of the azimuthal rotation angle ϕ, obtained for the three dislocations, *A*–*C*, and the virtual line (denoted *D*) connecting the two outcrops of *A* and *B* shown in Fig. 2. The solid lines are the results of a fit to the transformation formula.

Table 1
Summary of the fitting parameters, α and β, and the configuration of the dislocation lines studied.

Dislocation	α	β	Orientation	Length
A, *B*	45°	−45°	[011]	*B*: 61 μm
C	53.3°	−71.6°	[123]	–
D†	0°	0°	[$1\bar{1}0$]	72 μm

† The virtual line connecting the two outcrops of *A* and *B* in Fig. 2.

and β, which represent, in the experiment, two Euler angles of the lines with respect to the (001) plane and the [$1\bar{1}0$] direction, respectively, are described in Table 1. From the fitting values, we determined the crystallographic orientations and the lengths of the lines in the sample. The results are summarized in Table 1. Dislocations *A* and *B* were both identified as the [011] direction, and their outcrops are aligned parallel to the [$1\bar{1}0$] direction, indicating that the dislocations are located in the ($\bar{1}\bar{1}1$) slip plane. Dislocation *C* was revealed to be parallel to the [123] direction, and it is still located in the same ($\bar{1}\bar{1}1$) slip plane. On the other hand, the length of dislocation *B* was found to be 61 μm, indicating that dislocation *B* runs down to a depth of 43 μm below the surface along the [011] direction and bends towards dislocation *C* in the same slip plane.

5. Conclusions

We have presented an X-ray topographic technique for characterizing the three-dimensional distribution of dislocations, based on using a symmetric reflection *via* azimuthal rotation of a sample. The results reported here indicate that the technique is a very useful tool for quantitative determination of the orientations and locations of dislocation lines in single crystals.

This research was supported by grants from the MOST (KOSEF) through the National Core Research Center for Systems Bio-Dynamics, from the Ministry of Commerce, Industry and Energy, from the Korea Industrial Technology Foundation (KOTEF), and from the KOFST through the Brain Pool project. Use of the Advanced Photon Source was supported by the US Department of Energy, Office of Science, Office of Basic Energy Sciences, under contract No. W-31-109-ENG-38.

References

Authier, A. (2001). *Dynamical Theory of X-ray Diffraction*. New York: Oxford University Press.
Haruta, K. (1965). *J. Appl. Phys.* **36**, 1789–1790.
Koch, A., Raven, C., Spanne, P. & Snigirev, A. (1998). *J. Opt. Soc. Am. A*, **15**, 1940–1951.
Lang, A. R. (1959*a*). *Acta Cryst.* **12**, 249–250.
Lang, A. R. (1959*b*). *J. Appl. Phys.* **30**, 1748–1755.
Lübbert, D., Baumbach, T., Härtwig, J., Boller, E. & Pernot, E. (2000). *Nucl. Instrum. Methods Phys. Res. Sect. B*, **160**, 521–527.
Ludwig, W., Cloetens, P., Härtwig, J., Baruchel, J., Hamelin, B. & Bastie, P. (2001). *J. Appl. Cryst.* **34**, 602–607.
Miltat, J. & Dudley, M. (1980). *J. Appl. Cryst.* **13**, 555–562.
Vreeland, T. Jr (1976). *J. Appl. Cryst.* **9**, 34–38.
Yuan, D. & Dudley, M. (1992). *Mol. Cryst. Liq. Cryst.* **211**, 51–58.